Tošić, N., Marinković, S., Pecić, N., Ignjatović, I., Dragaš, J., 2018. Long-term behaviour of reinforced beams made with natural or recycled aggregate concrete and high-volume fly ash concrete. Construction and Building Materials 176, 344–358. https://doi.org/10.1016/j.conbuildmat.2018.05.002

Long-term behaviour of reinforced beams made with natural or recycled aggregate concrete and high-volume fly ash concrete

Nikola Tošić[a,*], Snežana Marinković[a], Nenad Pecić[a], Ivan Ignjatović[a], Jelena Dragaš[a]

[a] *University of Belgrade, Faculty of Civil Engineering, Bulevar kralja Aleksandra 73, 11000 Belgrade, Serbia*

* Corresponding author. Tel.: +381 11 3218 547; fax: +381 11 3370 253.
E-mail address: ntosic@imk.grf.bg.ac.rs
Postal address: Faculty of Civil Engineering, Bulevar kralja Aleksandra 73, 11000 Belgrade, Serbia

Snežana Marinković
E-mail address: sneska@imk.grf.bg.ac.rs
Nenad Pecić
E-mail address: peca@imk.grf.bg.ac.rs
Ivan Ignjatović
E-mail address: ivani@imk.grf.bg.ac.rs
Jelena Dragaš
E-mail address: jelenad@imk.grf.bg.ac.rs

ABSTRACT

Six simply supported reinforced concrete beams were tested under sustained loads for 450 days. The beams were made from natural aggregate concrete (NAC), recycled aggregate concrete (RAC) and high-volume fly ash concrete (HVFAC); two beams were made from each concrete and loaded after 7 and 28 days. On the beams, deflections, cracking and strains were measured while concrete specimens were used to determine physical-mechanical properties of concretes and measure shrinkage and creep. Results showed similar increases in deflections relative to initial deflections for all six beams. The results are also compared with code predictions and with existing results in literature.

Keywords:

recycled aggregate concrete; high-volume fly ash concrete; reinforced concrete; beam; deflection; creep; shrinkage

1. Introduction

The research community has been investigating possible solutions to environmental issues of concrete production. As the world's most-used construction material, almost 20 billion tons of concrete are produced annually worldwide [1]. This huge amount of concrete requires equally large amounts of its component materials: 15 billion tons of aggregates (river or crushed stone) [2] and 4.2 billion tons of cement [3]. Although concrete has a low embodied energy compared with other materials, the scale of its use means a significant impact on the environment.

The first impact is through the production of cement. Using current practice, each kg of cement produced is associated with an average of 842 g of CO_2; taking into account global annual cement production, the cement industry is actually responsible for 7–10% of all anthropogenic CO_2 emissions [4]. The second significant impact of concrete is its end-of-life, i.e. what happens after any concrete, plain or reinforced, has been decommissioned and demolished. Currently, most of it is still simply landfilled. What remains after the demolition of concrete structures is construction and demolition waste (CDW): in the EU alone, around 850 million tons of CDW are generated annually, accounting for approximately 30% of total waste generated [5].

One promising solution for these problems is the recycling of CDW to produce recycled aggregates in order to replace river or crushed stone aggregates in concrete production. This approach has the benefit of saving natural resources and reducing the amount of CDW being landfilled. A second potential solution is the partial replacement of cement by supplementary cementitious materials, usually industrial by-products. This approach both saves natural resources but also reduces the use (and indirectly production) of cement, thus potentially lowering CO_2 emissions.

As for recycling CDW, it can be performed on several materials, such as masonry and concrete. When concrete (plain or reinforced) is recycled, the produced aggregates are called recycled concrete aggregates (RCA). The content of other CDW (masonry, asphalt, glass, wood, etc.) must be kept very low, e.g. 10% [6]. Since concrete is composed of natural aggregates bound by hardened cement mortar, after crushing concrete waste, the final product, RCA, is composed of natural aggregate particles with some 'residual cement paste' bound to them. This 'residual cement

paste' is one of the defining characteristics of RCA and it influences most of its properties: RCA generally has lower density, higher porosity and greater water absorption compared with natural (both river and crushed stone) aggregates (NA) [7–9].

When RCA is used to produce concrete, this new concrete is called recycled aggregate concrete (RAC) and its use has been investigated for several decades [10]. So far, RCA has mostly found its way to use in applications such as road sub-base and non-structural concretes; only 1% of aggregates used in the production of structural concrete is RCA [11]. However, true recycling of CDW must lead to greater use of RCA in structural applications. In this study, RAC will refer to concrete in which only coarse aggregates (particle size > 4 mm) are replaced with RCA.

RAC has been very comprehensively investigated. The research on RAC has mostly focused on short-term mechanical and durability-related properties: compressive strength, tensile strength, modulus of elasticity, carbonation resistance, chloride ion penetration, etc. Comprehensive literature reviews analysing these properties of RAC compared with companion natural aggregate concrete (NAC)—usually defined as having the same water–cement (w/c) ratio—were published in recent years [12,13]. The general conclusion from these literature reviews is that mechanical properties of RAC with 100% replacement of coarse aggregate with RCA are, on average, lower than those of companion NAC (20–40% for compressive strength, 20% for tensile strength and 30% for the modulus of elasticity) [12,13].

A topic that has been less investigated is the shrinkage and creep behaviour of RAC. RCA exerts several influences on these properties in RAC: since RCA is usually weaker than NA, it provides less restraint for shrinkage and because of the residual cement paste on RCA particles, RAC usually has a larger total volume of cement paste compared with companion NAC leading to greater shrinkage and creep. Several literature reviews on studies of shrinkage and creep of RAC have been published [12,14,15]: studies covered in these literature reviews systematically found larger shrinkage and creep strains for RAC compared with companion NAC – for RAC with 100% replacement of coarse aggregates the increases in shrinkage and creep relative to companion NAC can be expected to be 20–50% and 20–60%, respectively.

One option for partial cement replacement is fly ash, a by-product of coal combustion in thermal power plants. Fly ash has pozzolanic properties and is produced globally in large quantities – 900–1000 megatons annually [4]. When fly ash is used in the production of concrete in which it constitutes more than 50% of total cementitious materials, then such a concrete is called high-volume fly ash concrete (HVFAC) [16]. For HVFAC, studies are less comprehensive and more difficult to methodologically carry out because fly ash is a by-product of coal combustion and its physical properties can vary considerably, depending on the coal from which it originated and the technological process employed in the thermal power plant. The properties of fly ash with the greatest influence on HVFAC properties are the particle size distribution and chemical composition. The mean particle size of fly ash can vary from 1 to 100 μm, with a typical size of around 20 μm [17]. One possible distinction between different types of fly ash is based on the criterion of the American standard ASTM C618-12 [18]: if the sum of silicon, aluminium and iron oxides in fly ash is greater than 70%, the fly ash is defined as class F, otherwise as class C.

One literature review available for HVFAC has been published recently [17]. For compressive strength, HVFAC with 45–55% of fly ash in total cementitious materials on average has around 60% of the compressive strength of companion NAC produced with the same water–cementitious materials ratio (w/cm) after 28 days and around 75% after 90 days [17]. Reductions were also found in tensile strength and modulus of elasticity: 35–45% reductions for HVFAC with 45–55% of fly ash in total cementitious materials; the decrease in the modulus of elasticity was found to be between 10% and 60% [17].

The effect of fly ash on shrinkage is mostly beneficial: literature review revealed that drying shrinkage of HVFAC can be reduced up to 50% for fly ash contents of 50% of total cementitious materials [17]. The lower shrinkage of HVFAC compared with companion NAC was also explained as a result of reduced cement paste content and a lower amount of hydrated paste (caused by the slower pozzolanic reaction) [19]. For creep, similar trends can be expected. When comparing HVFAC and companion NAC proportioned to have the same strength at the time of loading, HVFAC will exhibit lower creep due to the larger increase in compressive strength [20].

As stated earlier, in order to achieve the full potential of both RAC and HVFAC, they have to find their way to use in structural applications. There are a considerable number of studies investigating the structural behaviour of these two concrete. The most numerous are studies testing the ultimate flexural and shear strength of RAC [21–26] and HVFAC [27–29] beams; in the case of RAC, there are even studies on structures, such as static pushover or dynamic shake-table tests [30,31]. For RAC and HVFAC structural members, the studies generally don't find any significant difference in ultimate loads compared with companion NAC members. However, for both concretes, differences are found compared with companion NAC in terms of cracking and deflections. Because of weaker aggregates in RCA, cracking and short-term deflections are greater for RAC members compared with companion NAC members [22,23]; for HVFAC members, authors noted no significant differences compared with companion NAC or even lower short-term deflections and less cracking [28,29].

A topic that has been much less researched is the long-term behaviour of reinforced RAC and HVFAC members under sustained loads even though the need for taking their different long-term behaviour into account in design has been recognized [32]. The problem of serviceability, namely deflections, of reinforced concrete structures is often overlooked but not unimportant [33,34]: controlling appearance, preventing damage to non-structural elements and loss of utility are strong reasons for not disregarding this issue. However, because of the difficulty of adequately carrying out such tests and because of many factors which influence deflections, these tests are not numerous, even for NAC [35,36].

There is only a small number of long-term tests on reinforced RAC beams [21,37–42] and no tests on HVFAC beams. Unfortunately, many of the studies on RAC beams are published in the form of conference proceedings and often do not offer sufficient information. The studies vary in properties of used RCA (with water absorption from 1.9% to 6%), geometric properties of the beams (spans 2000–3700 mm, beam height 200–300 mm, reinforcement ratio 0.5–1.6%) and duration of sustained load (118–1000 days). The authors generally find larger deflections and greater cracking in RAC beams compared with companion beams produced from NAC with an identical w/c ratio as RAC [38,40,41]. Although some authors also test the applicability of existing design code provisions

for deflections [43,44] to RAC beams [40], the existing number of experimental results is not sufficient for conclusive remarks.

The objective of this research is, therefore, to investigate the long-term behaviour of reinforced NAC, RAC and HVFAC beams under sustained loads. This study aims to add new results of tests on RAC beams to a very limited existing database and obtain first-ever results on HVFAC beams – to start work in this area. The methodology selected for this investigation is the comparison of the behaviour of RAC and HVFAC beams with that of companion NAC beams.

For this purpose, three concrete mixtures were designed: NAC, RAC with 100% coarse aggregate replacement with RCA and HVFAC in which the cement-to-fly ash ratio was 1:1. From these mixtures, six 3.2 m-span, simply supported reinforced concrete beams were prepared (two from each mixture) and tested in four-point bending under sustained load for 450 days. All of the beams had identical geometry and reinforcement ratios, while from each mixture one beam was loaded after 7 and another after 28 days. In order to simulate a realistic situation for structural members loaded at early ages, the beams were loaded to high stress-to-strength at loading age ($\sigma_c/f_{cm}(t_0)$) ratios: beams loaded after 7 days had a $\sigma_c/f_{cm}(t_0)$ ratio equal to 0.6, while beams loaded after 28 days had this ratio equal to 0.45.

Both of these ratios represent relatively high stress levels for reinforced concrete structures, although not forbidden – the $\sigma_c/f_{cm}(t_0)$ ratio of 0.6 is the stress limit for the characteristic load combination in Eurocode 2 (EC2) and *fib* Model Code 2010 (MC10) [44,45] (for all stress levels below this, no longitudinal cracking should be expected). However, design of structural members according to ultimate limit state (ULS) requirements can easily lead to high stress levels in service.

This gives rise to the problem of creep non-linearity. It is a common understanding that below $\sigma_c/f_{cm}(t_0)$ ratios of 0.4–0.5, creep strain is linearly related to stress. Above this limit, the relationship becomes non-linear, mostly a consequence of damage induced by time-dependent growth of micro-cracks [46]. Since the primary interest in analysing the long-term behaviour of reinforced concrete members is their serviceability behaviour, viz. deflections, non-linear creep behaviour poses a challenge to their design.

Since creep non-linearity is caused by cracking and micro-cracking damage, one approach to serviceability analysis is the incorporation of creep with aging and shrinkage into microplane modelling of cracking damage, because the microplane model for concrete is already embedded in various nonlinear softwares (e.g. ATENA, DIANA) [46]. Mazzotti and Savoia [47] have proposed a model which combines the effects of cracking damage and creep modelled by a modified version of solidification theory, for uniaxial compression. These prediction models require a significant computational effort, i.e. it is adequate only for non-linear software.

On the other hand, standards like EC2 and MC10 introduce simplified procedures valid for certain stress levels [44,45]. These procedures present in fact the 'linearization' of nonlinear problem introducing the so-called nonlinear creep coefficient.

The general definition of creep strain can be taken as given by Ruiz et al. [48]:

$$\varepsilon_{cc}\left(t, t_0, \frac{\sigma_c}{f_c}\right) = \varepsilon_{ci}\left(t_0, \frac{\sigma_c}{f_c}\right) \cdot \varphi\left(t, t_0, \frac{\sigma_c}{f_c}\right) \tag{1}$$

where ε_{cc} represents the creeps train, ε_{ci} represents the instantaneous strain and φ is the creep coefficient. For linear creep, this relation becomes

$$\varepsilon_{cc}(t, t_0) = \varepsilon_{ci}(t_0) \cdot \varphi(t, t_0) \tag{2}$$

i.e., the creep coefficient is stress-independent. For non-linear creep and stress-strength ratios below 0.7 [48], it is experimentally verified that 'affinity hypothesis' applies – linear and non-linear creep strains are related through the stress-strength ratio [45,48]. Hence, Eq. (1) can be expressed as

$$\varepsilon_{cc}\left(t, t_0, \frac{\sigma_c}{f_c}\right) = \varepsilon_{ci}(t_0) \cdot \varphi_{lin}(t, t_0) \cdot \eta\left(\frac{\sigma_c}{f_c}\right) \tag{3}$$

where φ_{lin} is the linear, stress-independent creep coefficient and η is the 'affinity coefficient'. In that way the nonlinear creep coefficient is introduced as:

$$\varphi_{nonlin} = \varphi_{lin}(t, t_0) \cdot \eta\left(\frac{\sigma_c}{f_c}\right) \tag{4}$$

For instance, MC10 defines $\sigma_c/f_{cm}(t_0)$ = 0.4 as the limit up to which linear creep theories apply [45]. For stress levels up to $\sigma_c/f_{cm}(t_0)$ = 0.6, MC10 allows a simplified procedure with the application of a nonlinear creep coefficient defined as:

$$\varphi_\sigma(t,t_0) = \varphi(t,t_0) \cdot \exp\left[1.5 \cdot \left(\frac{\sigma_c}{f_{cm}(t_0)} - 0.4\right)\right] \quad (5)$$

where $\varphi_\sigma(t,t_0)$ is the nominal non-linear creep coefficient and $\varphi(t,t_0)$ is the linear creep coefficient calculated according to the MC10 model. The exponential function of the stress-strength ratio is adopted as the affinity coefficient η from Eq. (3). This non-linear creep coefficient is only an approximation, as is acknowledged by MC10, since it 'does not take into account the observation that non-linearity decreases with increasing duration of loading' [45]. Hence, predictions based on the application of a non-linear instead of a linear creep coefficient according to Eq. (5) should be on the safe side. This is a reasonable approach for any simplified procedure, which is more suitable for design purposes and engineering practice than complex non-linear software

Following the MC10 criteria, all six beams in the experiment were initially loaded up to stress levels which lead to non-linear creep behaviour (although the beams loaded after 28 days were only slightly above the limit). Beside presenting the design, execution and results of the experiment, an analysis of own experimental results and those of several other investigations is carried out in order to draw conclusions about the long-term behaviour of reinforced RAC and HVFAC beams under sustained loads. Also, the MC10 simplified approach is tested against own experimental results for all beams.

2. Experimental programme

2.1. Materials

The NA used in this study (sand and gravel) was a commercially available river aggregate from an excavation site on the Danube river in the vicinity of Belgrade. NA was obtained in three fractions: I (0/4 mm) – sand, II (4/8 mm) and III (8/16 mm) – gravel.

The RCA used in this study was obtained by demolishing an existing 40 year old highway bridge in the vicinity of Belgrade, Serbia. The aggregate was obtained by crushing columns and the deck of the bridge in a GIPO GISLER POWER construction site mobile recycling machine. The

demolished structure was relatively clean from impurities as the asphalt had been scraped of the deck prior to demolition. The aggregates were sieved into two fractions for testing: II (4/8 mm) and III (8/16 mm). Since very little was known about the original structure, Ø100/100 mm cores were taken from the columns and the deck of the bridge prior to demolishing and compressive strength was tested. The compressive strength of the cores taken from the bridge deck and from the column was 35 and 23 MPa, respectively (all values are average of three samples).

For both NA and RCA, oven-dry (OD) and saturated-surface dry (SSD) densities were determined according to methods given in EN 1097–6 [49]. Water absorption was tested for both NA and RCA after 24 h according to EN 1097–6 [49] but for RCA also after 30 min. The properties of the aggregates are provided in Table 1. The results show relatively moderate values for final (24 h) water absorption for RCA. Together with OD density values (which are approximately 10% lower compared with NA), this RCA can be classified as class B-I according to the classification proposed by Silva et al. [50]; this is actually a lower quality for recycled aggregates made only from concrete waste but still does not prevent them from being used in the production of RAC [50]. The 30 min water absorption values were 82% and 86% of the final value for fractions RCA II and RCA III, respectively.

The cement used in this study was commercially available CEM II Portland-composite cement produced by Lafarge Beočin, Serbia. The cement type was CEM II/A-M(S-L) 42.5R according to EN 197-1 [51]. The composition of this cement is 80–94% Portland cement clinker, 6–20% ground slag and limestone and 0–5% gypsum and mineral fillers and its specific density is 3050–3150 kg/m^3. The chemical composition of cement is given in Table 2.

The fly ash used in this study was obtained from the Nikola Tesla B power plant in Obrenovac, Serbia. The fly ash had a mean particle size of 8.53 μm determined using a Mlavern Instruments Mastersizer 2000 and a specific density of 2075 kg/m^3 determined according to ASTM C188-15 [52]. [52]. The chemical composition and physical properties were assessed by X-ray fluorescence analysis and the results are given in Table 2. As can be seen, the tested sample meets all of the requirements in the European standard EN 450-1 [53] and according to the loss on ignition it would

be classified as a category A fly ash. According to criteria in the American standard ASTM C618-12a [18] the fly ash would be classified as class F, i.e. low-calcium fly ash.

Two types of reinforcement were used in this study: (1) Ø10 mm ribbed bars were grade B500C with a yield stress of f_y =574–600 MPa and ultimate strain ε_u = 10.4–12.6% and (2) Ø6 mm plain bars were grade SAE1108 with a yield stress of f_y =395 MPa and ultimate strain ε_u = 32%.

2.2. Mixture design, casting and curing of beams and specimens

Three concrete mixtures were designed with a target 28-day compressive strength of 35 MPa on a 100 mm cubic sample and a 100–150 mm initial slump:

- NAC
- RAC with 100% coarse RCA
- HVFAC with a cement-to-fly ash ratio 1:1

The mixture proportions are given in Table 3. It should be noted that for RAC, additional water was added for the absorption of RCA. The amount of additional water used was slightly smaller than necessary for the measured 30 min absorption, and was determined through trial mixtures and testing workability. The choice of compensating the 30 min absorption was made based on the usual transport duration for ready-mixed concrete in Belgrade and the target of maintaining workability during these 30 min. No admixtures were added to any of the mixtures. The mixing procedure was similar for all three mixtures: (1) sand and coarse aggregates were mixed for approximately 1min, (2) cement (and fly ash) were added and mixed with aggregates for 1 min, (3) total water was added during 30 s and (4) the concrete was mixed for another 2.5 min; the overall mixing time was 5 min.

Concrete compressive strength (f_c) was tested on 100 mm cubes, splitting tensile strength ($f_{ct,sp}$) on Ø150/150 mm cylinders, flexural tensile strength ($f_{ct,fl}$) on 120/120/360 mm prisms and the modulus of elasticity (E_c) on Ø150/300 mm cylinders. Shrinkage and creep were measured on 120/120/360 mm prisms.

The reinforced concrete beams were designed upon consideration of previously published studies [35]. Taking into account the most usual dimensions of the tested specimens, a choice was

made to produce simply supported beams with a 3.2 m span and a *b/h* = 160/200 mm cross-section (span-to-height ratio *L/h* = 20) and load them in four-point bending in thirds of the span, Fig. 1. The beams were reinforced with 2Ø10 mm bars as bottom reinforcement (reinforcement ratio ρ = 0.58%) and with 2Ø6 mm bars as top reinforcement (reinforcement ratio ρ' = 0.21%). The reinforcement layout is given in Fig. 2.

Two beams were cast from each concrete mixture, one to be loaded after 7 and the other after 28 days. These loading ages were selected as being representative of 'early' and 'standard' loading ages of reinforced concrete structures. Depending on the concrete mixture and loading age, the beams were labelled NAC7, NAC28, RAC7, RAC28, HVFAC7 and HVFAC28. The beams were cast in wooden formwork in the Laboratory for Concrete and Rheology at the University of Belgrade's Faculty of Civil Engineering. Each beam was cast using approximately four batches of concrete; to aid placing, a 50 mm diameter vibrator was used to homogenize the concrete and release entrapped air.

After casting, the beams were cured for 24 h. During this period, they were covered with jute matting which was kept wet and above which plastic sheets were placed. After 24 h, one side of the formwork was opened and the beams were slightly moved to separate them from the other side of the formwork; thus, they were left lying on the bottom side of the formwork, drying under laboratory conditions. The accompanying concrete test specimens were cured in the same way. Curing concrete for only one day is standard practice in the Serbian construction industry, at least for the majority of structures such as buildings, and the aim was to simulate this in the experiment.

The laboratory in which the experiment was carried out was maintained under an average temperature of 21°C; however, relative humidity (RH) could not be controlled in a narrow range, its average value was 48%. The ambient conditions in the laboratory during the experiment are given in Fig. 3.

2.3. Test setup and procedure

When designing the sustained load for the beams, a fixed stress-to-strength at loading age ratio ($\sigma_c/f_{cm}(t_0)$) was chosen for all beams loaded at the same age. As already stated, for the beams

loaded after 7 days (NAC7, RAC7, HVFAC7), this ratio was adopted as 0.60, and for the beams loaded after 28 days (NAC28, RAC28, HVFAC28), this ratio was chosen as 0.45.

On the day of its loading, each beam was manually raised onto a steel support structure. After this, two steel Π-shaped rectangular tubes were placed on the beams in thirds of the span. Underneath each beam, a steel cart was driven and loaded with dead load consisting of concrete blocks obtained by cutting reinforced concrete beams from a previous experimental programme. The steel cart was aligned with the Π-shaped steel tubes and raised using manual jacks. Following this, bolts were screwed to connect the cart and steel tubes and the manual jacks were released, thus instantaneously applying the load, Fig. 4.

On each beam, deflections were measured using seven dial indicators: above the supports, in the middle of the shear spans, in the thirds of the span and in the middle of the flexural span. The first reading was taken after positioning the load beneath the beam and the instantaneous deflection was taken as the reading 5 min after load application. Afterwards, deflections were measured daily during the first week, weekly during the first month and monthly until 450 days after loading. Strains were measured using a mechanical strain gauge with a 100 mm base. Steel pins for measuring strains were glued onto the concrete surface 3 mm from the top fibre and 31 mm from the bottom fibre (at the level of bottom reinforcement). In the middle of the flexural spans, steel pins were also glued at 115 and 155 mm from the bottom fibre in order to measure the strain distribution along the cross-section height, a detail of this is given in Fig. 5. Strains were measured at the same as deflections. Finally, cracks were monitored, viz. crack spacing and width. A first inspection of each beam was performed after raising it on supports. Subsequently, 1 h after loading, cracks were measured in detail; their position and lengths were identified and highlighted with a marker and their widths were measured using a crack gauge. Further measurements were performed 7, 28, 90, 180, 365 and 450 days after loading.

Shrinkage was measured on three 120/120/360 mm prisms for each mixture. The prisms were taken out of the moulds 24 h after casting and held in the upright position. Immediately afterward, steel pins for strain measurements were glued on the concrete surface of two opposite sides of each prism; measurements began approximately 1 h after unmoulding. Thus, all reported shrinkage

values are averages of six measurements. The same mechanical strain gauge was used as for strain measurements on beams.

Creep was tested in steel frames using a lever system on groups of three 120/120/360 mm prisms, Fig. 6. Unfortunately, due to equipment restrictions of the laboratory, only four frames were available. Hence, creep was tested on RAC and HVFAC by loading three prisms at the same time as the beams: after 7 and after 28 days (RAC7, RAC28, HVFAC7 and HVFAC28). The prisms were loaded to an identical $\sigma_c/f_{cm}(t_0)$ ratio as the beams: 0.60 and 0.45 for the prisms loaded after 7 and 28 days, respectively. Steel pins for mechanical strain gauge measurements were glued on all four sides of each prism. Thus, every reported creep value is an average of 12 measurements.

3. Experimental results

3.1. Concrete properties

Properties of the concrete mixtures in the fresh and hardened state are given in Table 4. The slump values given in Table 4 show that without a plasticizer, it was relatively difficult to control the workability of RAC and HVFAC mixtures. As for the 28-day compressive strength, both NAC and RAC slightly overshot the target 35 MPa with NAC having a 9% higher compressive strength compared with RAC. HVFAC was 14% below the target and, importantly, the increase in strength after 28 days was not significant. At first look, this is in contrast with previous findings, as the increase in strength after 28 days is one of the most highlighted aspects of HVFAC [16,17]; in this study the increase from 28 to 90 days was 14.6% for HVFAC, nonetheless larger than the 3.7% increase for NAC. However, this was caused by the curing regime of only 24 h of wet curing, which significantly slowed down and decreased the development of compressive strength [54].

NAC also had the highest modulus of elasticity, 5% and 12% greater compared with RAC and HVFAC, respectively. It should be noted that due to equipment problems, the reported 28-day value for RAC is a single measurement whereas all others are averages of three specimens. For tensile strength, both splitting and flexural, NAC and RAC have practically identical values whereas HVFAC has a somewhat lower strength, especially after 7 days.

Results of shrinkage measurements are given in Table 5 and Fig. 7. As seen from the results, RAC had the largest shrinkage strain after 477 days, 21% greater than NAC, whereas HVFAC

displayed the lowest shrinkage strain, 7% smaller than NAC. Viewed in a logarithmic time scale in Fig. 7, the results display the typical lower inclination in early times with an increase in slope after approximately 10 days. However, the anticipated levelling-off of the shrinkage curve, indicating an approach to its final value is not yet detectable in any of the curves after 477 days.

As described earlier, creep was measured on RAC and HVFAC prisms loaded after 7 and 28 days (RAC7, RAC28, HVFAC7 and HVFAC28). The results are presented in Table 6 and Fig. 8. In Table 6, $\varepsilon_c(450)$ denotes the total strain measured on prisms for testing creep after 450 days, $\varepsilon_{ci}(t_0)$ is the initial strain measured 5 min after loading (loading ages of 7 and 28 days), $\varepsilon_{cs}(450)$ is the corresponding shrinkage strain measured reported in Table 5 and $\varepsilon_{cc}(450)$ is the creep strain after 450 days, obtained by subtracting the initial and shrinkage strains from the total strain. Also reported in Table 6 are the stresses in the prisms $\sigma_c(t_0)$, the stress-to-strength at loading age ratios $\sigma_c/f_{cm}(t_0)$, and the experimental creep coefficient after 450 days $\varphi_{exp}(450)$ calculated as

$$\varphi_{exp} = \frac{\varepsilon_{cc}(t)}{\varepsilon_{ci}(t_0)} \tag{6}$$

Since all of the prisms were loaded to high stress levels, as previously explained, the reported experimental creep coefficient is in fact the non-linear creep coefficient. The experimental creep coefficient can still be defined using Eq. (1), however it is stress-dependent and represents the product of linear creep coefficient and affinity coefficient according to Eq. (4).

Looking again at Table 6, interestingly, in this experiment practically identical experimental creep coefficients were obtained for both loading ages, for both RAC and HVFAC. Different loading age and different stress-to-strength at loading age ratio didn't cause significant difference in experimental creep coefficient within the same concrete type, possibly pointing to a higher limit of linear creep than 0.4 of compressive strength under circumstances as in this investigation. Similar to shrinkage, RAC displayed a significantly more pronounced creep behaviour compared with HVFAC: the RAC creep coefficient was 45% and 60% greater compared with HVFAC for specimens loaded after 7 and 28 days, respectively.

In Fig. 8, the stress-dependent strains $\varepsilon_{c\sigma}(t,t_0) = \varepsilon_{ci}(t_0) + \varepsilon_{cc}(t)$ are plotted in a logarithmic time scale..For HVFAC, the values for the two loading ages lie on parallel lines, reflected in the

practically identical experimental creep coefficients, whereas for RAC the gap between the lines slowly decreases, also reflected by the experimental creep coefficient being slightly larger for the loading age of 28 days, contrary to initial expectations.

3.2. Results on reinforced concrete beams

After measuring the mechanical properties of the concretes, the load for each beam was calculated so that the target $\sigma_c/f_{cm}(t_0)$ ratios could be achieved. Table 7 lists, for each beam, the total imposed bending moment M_{tot}, the cracking moment M_{cr}, the ultimate bending moment M_{ult}, and the ratios M_{tot}/M_{cr} and M_{tot}/M_{ult}. The cracking moment for each beam was calculated as

$$M_{cr} = W_i \cdot f_{ctm}(t_0) \tag{7}$$

where W_i is the section modulus of the transformed cross-section and $f_{ctm}(t_0)$ is taken as $f_{ct,sp}(t_0)$ as per MC10 [45]. The ultimate bending moment is calculated as

$$M_{ult} = A_{s1} \cdot f_y \cdot d \cdot (1 - 0.513 \cdot \frac{A_{s1} \cdot f_y}{b \cdot d \cdot f_{cm}}) \tag{8}$$

where A_{s1} is the area of tensile reinforcement, f_y is the nominal reinforcement yield strength, d is the cross-section effective depth, b is the cross-section width and f_{cm} is the 28-day concrete compressive strength (converted to standard cylinder strength using a conversion factor 0.75).

It can be seen from Table 7 that the M_{tot}/M_{cr} ratios are very similar among beams loaded at the same age and that the imposed load is significantly greater than the cracking load. From the M_{tot}/M_{ult} ratios it can be seen that the NAC and RAC beams were loaded to 0.44–0.55 of their ultimate load, which is a relatively usual service load level. At the same time, the M_{tot}/M_{ult} ratios are smaller for HVFAC beams as a consequence of their lower compressive strength compared with NAC and RAC.

Results of mid-span deflection measurements on the beams are given in Table 8 and in Fig. 9, grouped by loading age; $a(t_0)$ represents the initial deflection measured 5 min after applying the imposed load and $a(t–t_0)$ represents the long-term deflection after $t–t_0$ days under load. It is worth noting that the measured deflections do not include only the deflections of the beam from self-weight, approximately 0.30 mm. The absolute values of deflection in Table 8 vary in a wide range

and because the beams were loaded to different loads and had different compressive strengths they can be compared only in a normalised, i.e. dimensionless form.

Therefore, the last column in Table 8 presents the normalised deflection $a(450)/\ a(t_0)$, i.e. the final long-term–to–initial deflection ratio. It can be seen that for all six beam, regardless of the concrete type or loading age, this ratio is in a narrow range of 2.03–2.36, i.e. all the ratios differ by no more than 15%. The complete time evolution of the $a(t–t_0)/\ a(t_0)$ ratio is shown in Fig. 10, again grouped by loading age and in logarithmic time scale. The normalised deflections evolve practically identically in all the beams except for beam RAC28. This is a significant result considering the differing parameters in the six beams. On one hand, for beams made from the same concrete and loaded at different ages, no effect of loading age and stress level can be observed; this result is supported by creep measurements on RAC and HVFAC prisms in which there were no significant differences between prisms loaded after 7 and 28 days. Hence, it is plausible that for the conditions in this study, creep non-linearity is negligible up to $\sigma_c/f_{cm}(t_0) = 0.6$. On the other hand, differences in the evolution of normalised deflections are negligible between beams made from different concretes even though it was shown at the material level that they exhibit different shrinkage and creep behaviour. The reason for this is probably the relatively high M_{tot}/M_{ult} ratio applied to the beams, i.e. load level, which caused significant cracking in the beams. This lead to a relatively small height of the compressed zone in the beams' cross-section and consequently, the different effects of NAC, RAC and HVFAC creep and shrinkage are indistinguishable.

Strain measurements, taken with the mechanical strain gauge did not include shrinkage strain up to loading nor mechanical strain caused by self-weight of the beam. Measured tensile strains at the level of bottom reinforcement (ε_{s1}) and compressive strains 3 mm from the top fibre (ε_c), for the mid-span cross-section (Fig. 5) are given in Table 9. The reported values for each beam are averages of six measurements (three on each side of the beams, Fig. 5), i.e. they represent average strain over a length of 300 mm.

The compressive strain in concrete increased between 2.95 and 3.48 times and the tensile strain at the level of bottom reinforcement between 1.18 and 1.53 times with no clear correlation to loading age (stress level) or concrete type. Although, theoretically there should be only a small

increase in tensile steel strain over time, its larger occurrence here is the consequence of the measurement method: strain was measured on the concrete surface at the level of tensile reinforcement; hence, the increase in strain over time can be explained by the loss of concrete tension stiffening between two measurement points.

The measured strain distribution over the cross-section height is given in Fig. 11 for beams loaded after 7 and 28 days, respectively. As stated previously, the reported values are average strains over a length of 300 mm. Since the flexural span of the beams is under a constant bending moment, the average strain values represent a constant strain distribution (across the beam length) which is equivalent to the actual strain distribution (which is varying across the beam length). It can be seen that this 'equivalent' strain distribution is approximately linear during the entire 450 days for all beams thus confirming the validity of the standard plain section assumption used in the linear theory of beams as an adequate substitute for the actual strain distribution which significantly simplifies calculations. Similar results were obtained by other researchers for both NAC and RAC beams and lower stress-to-strength ratios [40,55].

All of the beams display a lowering of the neutral axis over time which is slightly more pronounced in beams loaded after 7 days compared with companion beams loaded after 28 days; this is in accordance with previous findings [40,55]. The lowering of the neutral axis is a physical consequence of the linear strain distribution and the fact that over time, concrete compressive strain increases significantly, whereas reinforcement tensile strain increases only slightly; theoretically, this is represented by the effective modulus method [45]. According to these measurements, the average strain distribution over the cross-section height is approximately linear even for high stress levels as applied in this experiment. Lowering of the neutral axis was more pronounced in NAC and RAC beams compared with HVFAC, for both loading ages, because of the higher load levels they were exposed to.

Crack measurements are presented in Table 10: average crack spacing s_m is reported along with average crack widths w_m and the full range of crack widths w_{min}–w_{max}. Most of the crack propagation occurred between 7 and 90 days, both in terms of increasing crack widths and opening of new cracks. The crack patterns of the beams immediately after loading and after 450 days are

displayed in Fig. 12; new cracks which appeared after the initial ones are coloured blue. From Fig. 12, the much more pronounced cracking of NAC and RAC beams compared with HVFAC beams can be clearly seen, as well as the more pronounced cracking of beams loaded after 7 days compared with those loaded after 28 days, for all concrete types. RAC beams—under similar tensile steel stress as NAC beams—have smaller or similar crack spacing and somewhat smaller crack widths. HVFAC beams, in this experiment, under lower tensile steel stress levels compared with NAC, show significantly larger crack spacing and smaller crack widths.

All experimental results on concrete specimens and beams can be found in the form of raw data Excel sheets using Mendeley Data and doi 10.17632/86mvvjr65h.1 [56].

4. Discussion

4.1. Comparison with existing results from literature

It was explained in section 1.2 that long-term experiments of reinforced concrete members under sustained loads are not very common, even in the case of NAC beams. The most comprehensive database of experimental results on NAC beams was prepared by Espion [35] with 217 results from 29 experimental programmes. All of the tests in the database are simply supported beams and the majority of the tests (83.4%) were carried out on beams with a rectangular cross-section. It is therefore useful to compare the main parameters of own experimental investigation with the range of parameters covered by Espion's database [35]. For this purpose, a subset of the database [35] was selected, according to the following criteria:

- studies carried out after 1945;
- rectangular cross-section;
- deformed bars;
- four-point bending or uniformly distributed load;
- total imposed load causes cracking immediately after loading;
- compressive strength 20–50 MPa;
- cross-section height greater than 100 mm;
- span-to-depth ratio smaller than 40;
- loading age t_0 smaller than 90 days; and

- stress-to-strength at loading age ratio ($\sigma_c/f_{cm}(t_0)$) below 0.6.

From the original 217 results in the database, 78 results from 10 experimental programmes satisfied the criteria. The range of their test parameters and results in comparison to the values in own experiment (for NAC beams) is given in Table 11. From the table, it can be seen that the values of test parameters chosen in own experiment are well within the range of previous experiments, with parameters like span, depth, compressive strength and $a(t–t_0)/a(t_0)$ ratio being close to median values of the ranges. The reinforcement ratio, and loading age are closer to lower values in the database ranges and the M_{tot}/M_{cr} ratio is closer to higher values in the database. Nonetheless, the chosen set of parameters fits into existing research.

For RAC beams, there are only two studies which provide sufficient data for comparison and analysis [40,41]. A comparison between test parameters and results for own RAC beams and those from previously published research [40,41] is given in Table 12; from the study by Seara-Paz [41], only beams with 50% and 100% coarse RCA replacement were considered (the replacement ratio of 20% was disregarded as too low). The beams in own experiment have a similar span to the ones from the two existing studies [40,41] but a smaller cross-section depth, reinforcement ratio and compressive strength. However, the RCA in this study had the lowest water absorption compared with RCA used in the other two experiments [40,41]. The load level, i.e. M_{tot}/M_{cr} and $\sigma_c/f_{cm}(t_0)$ ratio, is the highest in own experiment.

In general, all three experiments have a similar setup and design, but one important aspect is that in the study by Knaack and Kurama [40] beams from the 'UC' series were designed not to crack immediately after loading but after some time; these beams show a very large increase in deflections (because of their transition from uncracked to cracked state), hence, the large $a(t–t_0)/a(t_0)$ ratio obtained by Knaack and Kurama [40] (up to 7.4). Additional difficulties in comparing the results between the experiments are their different durations and $\sigma_c/f_{cm}(t_0)$ ratios. Two beams in Table 12 which are very similar are beam RAC28 and beam H65-100 from the study by Seara-Paz [41]: the beams are loaded to very similar $\sigma_c/f_{cm}(t_0)$ ratios, they have similar stiffness ratios and finally, their normalised deflections are similar, even though compressive strengths and

reinforcement ratios are different. Unfortunately, beside this observation, no definite conclusions can be drawn.

4.2. Comparison with code predictions

Finally, the measured deflections were compared with deflection predictions calculated according to the rigorous procedure of MC10 [45]. The rigorous procedure of MC10 is based on the interpolation of curvatures calculated in two states: (I) uncracked and (II) fully cracked state. The interpolation is performed at the cross-sectional level using a distribution coefficient ζ. For the case of pure bending, this distribution coefficient can be defined as

$$\zeta = \begin{cases} 1 - \beta \cdot \left(\frac{M_{cr}}{M}\right)^2 & \text{for } M \geq \sqrt{\beta} \cdot M_{cr} \\ 0 & \text{for } M < \sqrt{\beta} \cdot M_{cr} \end{cases} \tag{9}$$

where β is a coefficient accounting for the influence of the duration of loading or repeated loading and is taken as 1.0 for single short-term loading and 0.5 for sustained loads or multiple cycles of repeated loads [45]. Curvatures are then interpolated according to the following equation:

$$\left(\frac{1}{r}\right)_{eff} = \zeta \cdot \left(\frac{1}{r}\right)_{II} + (1 - \zeta) \cdot \left(\frac{1}{r}\right)_{I} \tag{10}$$

where $(1/r)_{eff}$ is the interpolated effective curvature, and $(1/r)_{II}$ and $(1/r)_{I}$ are curvatures in the fully cracked and uncracked states, respectively. The curvatures themselves are composed of a curvature due to load $(1/r)_{load}$ and curvature due to shrinkage $(1/r)_{cs}$. The curvature is calculated as

$$\left(\frac{1}{r}\right)_{n} = K \cdot \frac{M \cdot l^2}{E_{c,ef} \cdot I_{i,n}} + \varepsilon_{cs} \cdot \alpha_e \cdot \frac{S_{i,n}}{I_{i,n}}; \;\; n = I, II \tag{11}$$

where K is a coefficient depending on the static system (0.104 for a simply supported beam under uniformly distributed loading and 0.107 for a simply supported beam in four point bending in thirds of the span); $I_{i,n}$ is the moment of inertia of the transformed section in state I or II; $S_{i,n}$ is first moment of area of the reinforcement about the transformed section's centroid (in state I or II). The effect of creep is taken into account using the effective modulus of elasticity $E_{c,ef}$:

$$E_{c,ef} = \frac{E_{cm}}{1 + \varphi} \tag{12}$$

which also defines the modular ratio $\alpha_e = E_s/E_{c,ef}$ where E_s is the modulus of elasticity of reinforcement (may be taken as 200 GPa).

In this study, curvatures were calculated in 50 cross-sections for each beam and then a double numerical integration was performed to obtain deflections [57,58]. All the necessary input parameters (tensile strength, modulus of elasticity, shrinkage strain and creep coefficient) were calculated from measured values of concrete compressive strength using MC10 expressions [45]. Even though MC10 expressions are generally not directly applicable to RAC and HVFAC (mostly in terms of predicting shrinkage strain and creep coefficient), such an approach can still be useful when directly comparing the performance of MC10 expressions between NAC, RAC and HVFAC. Most of the differences in the MC10 model's behaviour between RAC and NAC can be expected to lie in material properties, since their structural behaviour, i.e. tension stiffening, has been shown to be similar [59]; unfortunately, for HVFAC no such studies were found.

Since the beams were loaded to high stress-to-strength at loading age ratios, non-linear creep effects had to be taken into account. As previously said, MC10 sets $0.4f_{cm}(t_0)$ as the limit up to which creep strain is linearly related to stress [45] and above this limit, up to stresses equal to $0.6f_{cm}(t_0)$, the simplified non-linear creep coefficient given by Eq. (5) is applicable. This approach has previously been successfully used to predict the deflections of beams loaded to high stress-to-strength at loading age ratios, even above $0.6f_{cm}(t_0)$ [60].

In this study, the calculation of deflections was carried out similar to the procedure described in the study by Mullem et al. [60]. After calculating the stress distribution at t_0, the non-linear creep coefficient was applied to the part of the cross-section which surpassed the linear creep limit of $0.4f_{cm}(t_0)$; this led to a cross-section consisting of reinforcement and 'two concretes': a less stiff concrete exposed to non-linear creep and a more stiff one under linear creep, as illustrated in Fig 13. However, in this analysis, the height of the compression zone at t_0 was approximately 40 mm for all six beams and the height of the zone under non-linear creep was approximately 11–15 mm for the beams loaded after 7 days and 4–5 mm for the beams loaded after 28 days. This led to a very small effect of non-linear creep on deflections, as reflected in the results in Table 8 where the $a(450)/a(t_0)$ were shown to be very similar for all six beams.

The results of the deflection calculation are shown in Fig. 14 (for clarity of presentation, the vertical axes do not start from 0). The results for NAC and RAC beam show a relatively good and acceptable agreement between measured and calculated values, with only deflections of beam NAC7 being significantly overestimated. Initial deflections are systematically overestimated, by 27.6% and 15.6% for beams NAC7 and NAC28, respectively and by 14.6% and 41.5% for beams RAC7 and RAC28 respectively. However, of much greater interest are deflections after 450 days which are overestimated by 12.8% for beam NAC7 and exactly predicted for beam NAC28, and overestimated by 2.4% and 8.8% for beams RAC7 and RAC28, respectively. In other words, the precision of predictions increases over time and final deflections are predicted with a maximal overestimation of experimental values of 13%, which can be considered as a good result. However, based on only this analysis it cannot be said whether the deflection predictions would be improved by taking into account different predictions of RAC properties compared with NAC. There is strong evidence that changes MC10 predictions, especially for creep and shrinkage, are necessary for application on RAC [14,15,61,62].

As for HVFAC beam, the results in Fig. 14 show a very significant overestimation of measured deflections by MC10. Qualitatively, the predicted deflection curve is appropriate but quantitatively it overestimates initial deflections by 39.8% and 88.9% for beams HVFAC7 and HVFAC28, respectively and final deflections by 44.2% and 71.3% for beams HVFAC7 and HVFAC28, respectively. Hence, the predictions remain significantly larger than measured values over time. Again, since these are the only results available on HVFAC beams, it cannot be claimed where the errors lie—whether in code expressions for material properties or structural behaviour of HVFAC, i.e. tension stiffening—more experimental results are necessary.

5. Conclusions

This study presented the results of an experimental programme testing the long-term behaviour of reinforced NAC, RAC and HVFAC beams under sustained load. Based on the results of tests on concrete specimens and reinforced concrete beams, the following conclusions are drawn:

1. RAC concrete with 100% coarse RCA, produced with the same effective w/c as companion NAC had an 8% lower 28-day compressive strength. HVFAC produced with a cement-to-fly ash ratio of 1:1 had a 26% lower 28-day compressive strength compared with NAC. The selected curing regime of only one day of wet curing significantly contributed to the lower compressive strength of HVFAC;
2. After 477 days, the unrestrained shrinkage strain of RAC and HVFAC, compared with NAC, was 22% greater and 8% smaller, respectively. The experimental creep coefficient of RAC and HVFAC specimens loaded after 7 days was practically identical to the creep coefficient of RAC and HVFAC specimens loaded after 28 days, even though specimens loaded after 7 days were loaded to a stress-to-strength at loading age ratio of 0.60 and specimens loaded after 28 days to a ratio of 0.45. However, the RAC creep coefficient was 45% and 60% greater compared with HVFAC for specimens loaded after 7 and 28 days, respectively;
3. Normalised deflections, i.e. the $a(t–t_0)/ a(t_0)$ ratio, after 450 days was in the range of 2.03–2.36 for all six beams, regardless of concrete type or loading age (stress level). No effect of creep non-linearity and loading age was observed between beams from the same concrete, as corroborated by results on concrete prisms. No effect of concrete type and different shrinkage and creep behaviour was observed between beams made from different concretes, possibly because of the high load level applied to the beams which caused significant cracking, a small height of the compressed concrete zone in the beams' cross-section and, consequently, an indistinguishable effect of different concrete types;
4. In line with previous findings, the cracking behaviour of RAC beams was more pronounced compared with NAC beams (crack spacing was smaller and crack widths larger), even though they were loaded to similar load levels. The crack pattern in HVFAC beams was much less developed, mostly because they were loaded to a lower load level. Between beams made from the same concrete, those loaded after 7 days displayed smaller crack spacing and larger crack widths than those loaded after 28 days, and developed more shrinkage-induced cracks over 450 days;
5. The experimental setup parameters used in this study fit well with previously executed experiments; therefore, comparison with own results is possible. For RAC beams, the results of

this study match very well the results of two previously published studies in terms of increase of normalised deflections. In this study, there was no significant difference in the increase of normalized deflections between RAC and NAC beams;

6. Experimental deflection curves for own beams were compared with MC10 predictions using code expressions to predict input parameters. For NAC and RAC beams good agreement was found between experimental and calculated values for final deflections, whereas initial deflections were overestimated. There was no significant difference between the performance of the MC10 model for deflections on NAC and RAC beams. The deflections of HVFAC are significantly overestimated, both initially and after 450 days (between 39.8% and 88.9%) pointing to significant differences in the MC10's performance of HVFAC compared with NAC and RAC. However, more experimental results are necessary for definite conclusions;
7. The results of this study are promising in terms of the applicability of RAC and HVFAC as structural concrete members under sustained loads. Only in this way, the full benefits of using these recycled and waste materials can be realized. Future research should focus on extending the experimental database with different basic parameters, especially with beams with T-cross sections, since this cross section type is more representative of reinforced concrete beams and can cause different beam's behaviour; finally research efforts should focus on providing analytical expressions for long-term material and structural properties of these concretes so that they can be designed using existing codes.

Acknowledgements

This work was supported by the Ministry for Education, Science and Technology, Republic of Serbia [grant number TR36017]; this support is gratefully acknowledged. The authors thank companies Čelikinvest, Deneza M and Gradient for material and equipment donations and Dr. Aleksandar Radević and Vedran Carević for help in carrying out tests described in this paper.

References

[1] WBCSD, The Cement Sustainability Initiative, World Bus. Counc. Sustain. Dev. (2009). http://www.wbcsdcement.org/pdf/CSIRecyclingConcrete-FullReport.pdf (accessed July 7, 2016).

[2] W.H. Langer, L.J. Drew, J.J. Sachs, Aggregate and the Environment, Alexandria, VA, 2004. www.agiweb.org/environment/publications/aggregate.pdf.

[3] USGS, Minerals Yearbook, US Geol. Surv. (2015).

minerals.usgs.gov/minerals/pubs/commodity/cement/mcs-2015-cement.pdf (accessed July 7, 2016).
[4] K.L. Scrivener, J.M. Vanderley, E.M. Gartner, Eco-efficient cements: Potential, economically viable solutions for a low-CO2, cement based materials industry, Paris, 2016.
[5] C. Fisher, M. Werge, EU as a Recycling Society, ETC/SCP Work. Pap. 2. (2011). scp.eionet.europa.eu/wp/ETCSCP 2per2011 (accessed July 7, 2016).
[6] EN 12620, Aggregates for concrete, CEN, Brussels, 2010.
[7] J. Xiao, J. Li, C. Zhang, Mechanical properties of recycled aggregate concrete under uniaxial loading, Cem. Concr. Res. 35 (2005) 1187–1194. doi:10.1016/j.cemconres.2004.09.020.
[8] K. Rahal, Mechanical properties of concrete with recycled concrete aggregates, Build. Environ. 42 (2007) 407–415.
[9] L. Evangelista, J. de Brito, Mechanical behaviour of concrete made with fine recycled concrete aggregates, Cem. Concr. Compos. 29 (2007) 397–401.
[10] P.J. Nixon, Recycled concrete as an aggregate for concrete - a review, Mater. Struct. 11 (1978) 371–378.
[11] FIB Task Group 3.3, Environmental design, FIB Bull. 28 (2004) 80.
[12] R.V. Silva, Use of recycled aggregates from construction and demolition waste in the production of structural concrete, Universidade de Lisboa, 2015.
[13] I. Ignjatović, Ultimate strength of reinforced recycled concrete beams, University of Belgrade, 2013.
[14] C.Q. Lye, R.K. Dhir, G.S. Ghataora, H. Li, Creep strain of recycled aggregate concrete, Constr. Build. Mater. 102 (2016) 244–259. doi:10.1016/j.conbuildmat.2015.10.181.
[15] C. Lye, G.S. Ghataora, R.K. Dhir, Shrinkage of recycled aggregate concrete, in: Struct. Build. Proc. Inst. Civ. Eng., ICE, 2016: pp. 1–25. doi:10.1680/jstbu.15.00138.
[16] J. Dragaš, I. Ignjatović, N. Tošić, S. Marinković, Mechanical and time-dependent properties of high-volume fly ash concrete for structural use, Mag. Concr. Res. 68 (2016) 632–645.
[17] A.M. Rashad, A brief on high-volume Class F fly ash as cement replacement - A guide for Civil Engineer, Int. J. Sustain. Built Environ. 4 (2015) 278–306. doi:10.1016/j.ijsbe.2015.10.002.
[18] ASTM-C618-12a, Standard specification for coal fly ash and raw or calcined natural pozzolan for use in concrete, ASTM International, West Conshohocken, PA, 2012.
[19] C.D. Atiş, High-Volume Fly Ash Concrete with High Strength and Low Drying Shrinkage, J. Mater. Civ. Eng. 15 (2003) 153–156. doi:10.1061/(ASCE)0899-1561(2003)15:2(153).
[20] ACI Committe 232, Use of fly ash in concrete Reported by ACI Comittee 232, American Concrete Institute, Detroit, 1986. http://trid.trb.org/view.aspx?id=277673.
[21] R. Sato, I. Maruyama, T. Sogabe, M. Sogo, Flexural Behavior of Reinforced Recycled Concrete Beams, J. Adv. Concr. Technol. 5 (2007) 43–61. doi:10.4334/JKCI.2009.21.4.431.
[22] I. Ignjatović, S. Marinković, Z. Mišković, A. Savić, Flexural behavior of reinforced recycled aggregate concrete beams under short-term loading, Mater. Struct. 469 (2013) 1045–1059.
[23] A.B. Ajdukiewicz, A.T. Kliszczewicz, Comparative tests of beams and columns made of recycled aggregate concrete and natural aggregate concrete, J. Adv. Concr. Technol. 5 (2007) 259–273. doi:10.3151/jact.5.259.
[24] G. Fathifazl, A.G. Razaqpur, O. Burkan Isgor, A. Abbas, B. Fournier, S. Foo, Shear capacity evaluation of steel reinforced recycled concrete (RRC) beams, Eng. Struct. 33 (2011) 1025–1033. doi:10.1016/j.engstruct.2010.12.025.
[25] M. Arezoumandi, A. Smith, J.S. Volz, K.H. Khayat, An experimental study on shear strength of reinforced concrete beams with 100% recycled concrete aggregate, Constr. Build. Mater. 53 (2014) 612–620. doi:10.1016/j.conbuildmat.2013.12.019.
[26] I. Ignjatović, S. Marinković, N. Tošić, Shear behaviour of recycled aggregate concrete beams with and without shear reinforcement, Eng. Struct. 141 (2017) 386–401. doi:10.1016/j.engstruct.2017.03.026.
[27] M. Arezoumandi, J.S. Volz, Effect of fly ash replacement level on the shear strength of high-volume fly ash concrete beams, J. Clean. Prod. 59 (2013) 120–130. doi:10.1016/j.jclepro.2013.06.043.
[28] M. Soman, K. Sobha, Strength and Behaviour of High Volume Fly Ash Concrete, Int. J. Innov. Res. Sci. Eng. Technol. 3 (2014) 12416–12424.
[29] S.W. Yoo, G.S. Ryu, J.F. Choo, Evaluation of the effects of high-volume fly ash on the

flexural behavior of reinforced concrete beams, Constr. Build. Mater. 93 (2015) 1132–1144.
[30] J. Pacheco, J. De Brito, D. Soares, Destructive Horizontal Load Tests of Full-scale Recycled Aggregate Concrete Structures, ACI Struct. J. 112 (2015) 815–826.
[31] J. Xiao, C.Q. Wang, J. Li, M. Tawana, Shake-table model tests on recycled aggregate concrete frame structure, ACI Struct. J. 109 (2012) 777–786.
[32] G. Dobbelaere, J. de Brito, L. Evangelista, Definition of an equivalent functional unit for structural concrete incorporating recycled aggregates, Eng. Struct. 122 (2016) 196–208. doi:10.1016/j.engstruct.2016.04.055.
[33] Z.P. Bazant, M.H. Hubler, Q. Yu, Excessive Creep Deflection: An Awakening, Concr. Int. 33 (2011) 44–46.
[34] Z. Bazant, Q. Yu, G. Li, G. Klein, K. Vladimir, Excessive Deflections of Record-Span Prestressed Box Girder, Concr. Int. 32 (2010) 44–52.
[35] B. Espion, Long-Term Sustained Loading Test on Reinforced Concrete Beams, Université Libre de Bruxelles Service Génie Civile, Brussels, 1988.
[36] N. Pecić, Improved method for deflection control of reinforced concrete structures, Faculty of Civil Engineering, Belgrade University, 2012.
[37] I. Maruyama, Y. Oka, R. Sato, Time-dependent Behavior of Reinforced Recycled Concrete Beams, in: CONCREEP 7, 2005.
[38] A. Ajdukiewicz, A. Kliszczewicz, Long-term behaviour of reinforced-concrete beams and columns made of recycled aggregate, in: Fib Symp. Concr. Eng. Excell. Effic. June 8-10, 2011: pp. 479–482.
[39] W.-C. Choi, H.-D. Yun, Long-term deflection and flexural behavior of reinforced concrete beams with recycled aggregate, Mater. Des. 51 (2013) 742–750. doi:10.1016/j.matdes.2013.04.044.
[40] A.M. Knaack, Y.C. Kurama, Sustained Service Load Behavior of Concrete Beams with Recycled Concrete Aggregates, ACI Struct. J. 112 (2015) 565–578. doi:10.14359/51687799.
[41] S. Seara-Paz, Efect of long-term deformations in structural flexural performance and bond behaviour analysis of recycled concrete, Universidade de Coruna, 2015.
[42] A. Łapko, R. Grygo, Long term deformations of recycled aggregate concrete (RAC) beams made of recycled concrete, in: Mod. Build. Mater. Struct. Tech., Vilnius Gediminas Technical University, Vilnius, 2010: pp. 709–712.
[43] ACI 318-11, Building code requirements for structural concrete (ACI 318-11) and commentary, American Concrete Institute, Farmington Hills, MI, 2011.
[44] EN 1992-1-1, Eurocode 2: Design of concrete structures - Part 1-1: General rules and rules for buildings, CEN, Brussels, 2004.
[45] FIB, fib Model Code for Concrete Structures 2010, International Federation for Structural Concrete (fib), Lausanne, 2013. doi:10.1002/9783433604090.
[46] Z.P. Bažant, M. Jirasek, Creep and Hygrothermal Effects in Concrete Structures, Springer, Dordrecht, 2018.
[47] C. Mazzotti, M. Savoia, Nonlinear Creep Damage Model for Concrete under Uniaxial Compression, J. Eng. Mech. 129 (2003) 1065–1075. doi:10.1061/(ASCE)0733-9399(2003)129:9(1065).
[48] P.G. Ruiz, M.F., Muttoni, A. and Gambarova, Relationship between nonlinear creep and cracking of concrete under uniaxial compression, J. Adv. Concr. Technol. 5 (2007) 383–393.
[49] EN 1097-6, Tests for mechanical and physical properties of aggregates - Part 6: Determination of particle density and water absorption, CEN, Brussels, 2000.
[50] R.V. Silva, J. De Brito, R.K. Dhir, Properties and composition of recycled aggregates from construction and demolition waste suitable for concrete production, Constr. Build. Mater. 65 (2014) 201–217. doi:10.1016/j.conbuildmat.2014.04.117.
[51] EN 197-1, Cement - Part 1: Composition, specifications and conformity criteria for common cements, CEN, Bru, 2000.
[52] ASTM C188-15, Standard Test Method for Density of Hydraulic Cement, ASTM International, West Conshohocken, PA, 2015.
[53] EN 450-1, Fly ash for concrete - Part 1: Definition, specifications and conformity criteria, CEN, Brussels, 2012.
[54] A.A. Ramezanianpour, V.M. Malhotra, Effect of curing on the compressive strength, resistance to chloride-ion penetration and porosity of concretes incorporating slag, fly ash or

silica fume, Cem. Concr. Compos. 17 (1995) 125–133. doi:10.1016/0958-9465(95)00005-W.
[55] W.G. Corley, M.A. Sozen, Time-Dependent Deflections of Reinforced Concrete Beams, Journa Am. Concr. Inst. 63 (1966) 373–386.
[56] N. Tošić, S. Marinković, I. Ignjatović, J. Dragaš, V. Carević, Experimental measurements on the behaviour of reinforced NAC,RAC and HVFAC beams under sustained loads, Mendeley Data, v1. (2017). doi:10.17632/86mvvjr65h.1.
[57] A.W. Beeby, S. Narayanan, Designer's guide to Eurocode 2: Design of concrete structures, Thomas Telford, London, 2005.
[58] FIB Bulletin 52, Structural Concrete - Textbook on Behaviour, Design and Performance, International Federation for Structural Concrete (fib), Lausanne, 2010. doi:10.1017/CBO9781107415324.004.
[59] C. Santana Rangel, M. Amario, M. Pepe, Y. Yao, B. Mobasher, R.D. Toledo Filho, Tension stiffening approach for interface characterization in recycled aggregate concrete, Cem. Concr. Compos. 82 (2017) 176–189. doi:10.1016/j.cemconcomp.2017.06.009.
[60] T. Van Mullem, N. Reybrouk, P. Criel, L. Taerwe, R. Caspeele, Contemporary Analysis and Numerical Simulation of Revisited Long-Term Creep Tests on Reinforced Concrete Beams from the Sixties, in: High Tech Concr. Where Technol. Eng. Meet - Proc. 2017 Fib Symp., International Federation for Structural Concrete (fib), Lausanne, 2017: pp. 2802–2809.
[61] C.Q. Lye, R.K. Dhir, G.S. Ghataora, Elastic Modulus of Concrete Cast with Recycled Aggregates, Struct. Build. 169 (2016) 314–339. doi:10.4028/www.scientific.net/AMM.423-426.1006.
[62] R.V. Silva, J. de Brito, R.K. Dhir, Establishing a relationship between the modulus of elasticity and compressive strength of recycled aggregate concrete, J. Clean. Prod. (2015). doi:10.1016/j.jclepro.2015.10.064.

List of tables:

List of figures:

Table 1

Click here to download Table: Table_1.docx

Table 1. Physical properties of NA and RCA

Aggregate	OD density* (kg/m^3)	SSD density* (kg/m^3)	Water absorption	
			30 min (%)	24 h (%)
NA I	2570	2600	–	1.20
NA II	2550	2580	–	1.24
NA III	2590	2620	–	1.04
RCA II	2390	2480	3.01	3.67
RCA III	2360	2550	3.55	4.05

*density values are rounded to the nearest 10 kg/m^3

Table 2

Click here to download Table: Table_2.docx

Table 2. Chemical and physical properties of cement and fly ash

Property	Cement	Fly ash
SiO_2 (%)	21.04	58.24
Al_2O_3 (%)	5.33	20.23
Fe_2O_3 (%)	2.37	5.33
$SiO_2 + Al_2O_3 + Fe_2O_3$ (%)	–	83.80
TiO_2 (%)	–	0.45
CaO (%)	60.43	7.62
MgO (%)	2.43	2.01
P_2O_5 (%)	–	0.00
SO_3 (%)	3.55	2.21
Na_2O (%)	0.22	0.52
K_2O (%)	0.70	1.51
MnO (%)	–	0.03
LOI (%)	3.53	2.10
Fineness (>45 μm) (%)	–	11.71

Table 3

Click here to download Table: Table_3.docx

Table 3. Mixture proportions of the tested concretes

Concrete	m_c (kg/m^3)	m_w (kg/m^3)	Δm_w (kg/m^3)	m_{FA} (kg/m^3)	NA (kg/m^3)			RCA (kg/m^3)	
					0/4 mm	4/8 mm	8/16 mm	4/8 mm	8/16 mm
NAC	285	175	–	–	815	543	453	–	–
RAC	285	175	21.5	–	767	–	–	511	426
HVFAC	200	195	–	200	810	486	324	–	–

Table 4

Click here to download Table: Table_4.docx

Table 4. Properties of fresh and hardened concrete

Concrete	Properties of fresh concrete		Properties of hardened concrete									
	Density (kg/m^3)	Slump (mm)	f_{cm}[1] (MPa)			E_{cm} (GPa)		$f_{ct,sp}$ (MPa)		$f_{ct,fl}$ (MPa)	
			7 d	28 d	90 d	7 d	28 d	7 d	28 d	7 d	28 d
NAC	2340	115	32.9	40.7	40.7	30.1	32.2	2.0	2.4	5.6	6.7
RAC	2240	140	32.2	37.4	38.8	26.2	30.8[2]	2.0	2.5	5.4	6.4
HVFAC	2200	70	21.8	30.1	34.5	25.2	28.7	1.2	2.1	4.3	5.2

[1]compressive strength values are measured on 100 mm cubes
[2]single measured value

Table 5

Click here to download Table: Table_5.docx

Table 5. Shrinkage strain measurements

Concrete	$\varepsilon_{cs}(t,t_s)$ (‰)				
	7 d	28 d	96 d	186 d	477 d
NAC	–0.143	–0.342	–0.540	–0.557	–0.645
RAC	–0.155	–0.385	–0.583	–0.660	–0.782
HVFAC	–0.125	–0.315	–0.410	–0.492	–0.597

Table 6

Click here to download Table: Table_6_R1.docx

Table 6. Creep measurements

Concrete	$\varepsilon_c(450)$ (‰)	$\varepsilon_{cl}(t_0)$ (‰)	$\varepsilon_{cs}(450)$ (‰)	$\varepsilon_{cc}(450)$ (‰)	$\varphi_{exp}(450)$ (–)	$\sigma_c(t_0)$ (MPa)	$\sigma_c/f_{cm}(t_0)$ (–)
RAC7	–3.413	–0.775	–0.782	–1.856	2.395	14.50	0.60
RAC28	–2.849	–0.594		–1.473	2.480	12.78	0.45
HVFAC7	–2.345	–0.664	–0.595	–1.086	1.634	9.84	0.60
HVFAC28	–1.855	–0.493		–0.767	1.554	10.20	0.45

Table 7

Click here to download Table: Table_7_R1.docx

Table 7. Total imposed, cracking and ultimate bending moments and their ratios

Beam	M_{tot} (Nm)	M_{cr} (t_0) (Nm)	M_{tot}/ M_{cr} (t_0)	M_{ult} (Nm)	M_{tot}/ M_{ult}
NAC7	7628	2289	3.33	14379	0.53
NAC28	6836	2742	2.49		0.48
RAC7	7865	2157	3.65	14304	0.55
RAC28	6356	2593	2.45		0.44
HVFAC7	5491	1678	3.27	14080	0.39
HVFAC28	5352	2069	2.59		0.38

Table 8

Click here to download Table: Table_8.docx

Table 8. Time evolution of mid-span deflections

Beam	$a(t_0)$ (mm)	$a(t–t_0)$ (mm)					$a(450)/\ a(t_0)$ (–)
		7 d	28 d	90 d	180 d	450 d	
NAC7	9.17	12.44	14.42	16.35	17.23	18.79	2.07
NAC28	8.11	10.92	12.52	13.85	14.92	16.51	2.04
RAC7	10.89	14.43	16.90	19.12	20.39	22.47	2.06
RAC28	6.23	8.76	10.36	11.65	12.91	14.69	2.36
HVFAC7	6.13	8.75	10.04	10.79	11.33	12.45	2.03
HVFAC28	4.04	5.22	6.01	6.61	7.33	8.72	2.16

Table 9

Click here to download Table: Table_9_R1.docx

Table 9. Measured beam compressive and tensile strains

Beam	ε_c (‰)		ε_{s1} (‰)	
	t_0	*450 d*	*t_0*	*450 d*
NAC7	-0.547	-1.887	0.923	1.215
NAC28	-0.442	-1.305	0.965	1.323
RAC7	-0.660	-2.185	1.462	1.763
RAC28	-0.412	-1.432	0.600	0.920
HVFAC7	-0.380	-1.272	0.735	0.865
HVFAC28	-0.280	-0.893	0.473	0.687

Table 10

Click here to download Table: Table_10_R1.docx

Table 10. Crack spacing and crack widths

Beam	t_0			450 days		
	s_m (mm)	w_m (mm)	w_{min}–w_{max} (mm)	s_m (mm)	w_m (mm)	w_{min}–w_{max} (mm)
NAC7	134.3	0.05	0.05–0.05	115.8	0.10	0.03–0.15
NAC28	119.5	0.08	0.03–0.15	110.4	0.11	0.03–0.20
RAC7	102.0	0.06	0.03–0.08	97.4	0.09	0.03–0.15
RAC28	123.6	0.05	0.03–0.08	102.5	0.07	0.03–0.10
HVFAC7	145.4	0.04	0.03–0.08	125.9	0.08	0.03–0.15
HVFAC28	153.1	0.04	0.03–0.05	128.9	0.05	0.03–0.08

Table 11

Click here to download Table: Table_11_R1.docx

Table 11. Comparison of test parameters and results from reference [35] and own experiment (NAC beams)

Test parameter	Database in [35]	Own experiment
L (mm)	1829–6400	3200
h (mm)	120–340	200
L/d	10.7–39.9	18.9
f_{cm} (MPa)	21.4–39.6	30.5
ρ (%)	0.55–2.64	0.58
ρ' (%)	0–1.67	0.21
t_0 (days)	14–53	7–28
$t–t_0$ (days)	60–1734	450
M_{tot}/M_{cr}	1.12–4.07	2.49–3.33
$\sigma_c/f_{cm}(t_0)$	0.20–0.58	0.45–0.60
I_I/I_{II}^*	2.14–7.18	5.19–5.61
$a(t–t_0)/a(t_0)$	1.62–3.82	2.04–2.07

*ratio of transformed section moments of inertia in uncracked (I) and fully cracked state (II)

Table 12

Click here to download Table: Table_12_R1.docx

Table 12. Comparison of test parameters and results from references [40,41] and own experiment (RAC beams)

Investigation	Beam	RCA (%)	RCA w.a.*	L (mm)	h (mm)	f_{cm} (MPa)	ρ (%)	t_0 (days)	$t–t_0$ (days)	M_{tot}/M_{cr}	$\sigma_c/f_{cm}(t_0)$	I_I/I_{II}	$a(t–t_0)/a(t_0)$
Own experiment	RAC7	100	3.67–4.05	3200	200	28.1	0.58	7	450	3.75	0.60	5.08	2.06
	RAC28	100						28		2.52	0.45	5.49	2.36
Knaack and Kurama [40]	UT-50-28	50	6.06	3700	230	43.6	1.32	28	119	0.91	0.12	3.05	5.91
	UT-50-7	50				40.2		7		1.18	0.16	2.76	7.40
	UC-50-28	50				49.6		28		0.81	0.10	3.21	5.47
	UC-50-7	50				43.6		7		1.08	0.14	2.87	7.13
	CC-50-7	50				40.0		7		2.41	0.31	2.82	3.12
	UT-100-28	100				41.4		28		0.94	0.13	3.01	5.96
	UC-100-28	100				48.2		28		0.83	0.10	3.19	6.12
	UC-100-7	100				40.6		7		1.14	0.15	2.83	6.00
	CC-100-28	100				43.8		28		1.85	0.24	3.12	2.40
	CC-100-7	100				38.5		7		2.5	0.32	2.80	3.19
Seara-Paz [41]	H50-50	50	5.40	3400	300	51.8	0.81	42	1000	1.95	0.31	5.28	1.79
	H50-100	50				42.9				2.40	0.39	5.03	2.24
	H65-50	100				42.2	0.86			1.85	0.32	5.67	1.94
	H65-100	100				32.4				2.41	0.43	5.30	2.47

*water absorption

Figure 1

Click here to download high resolution image

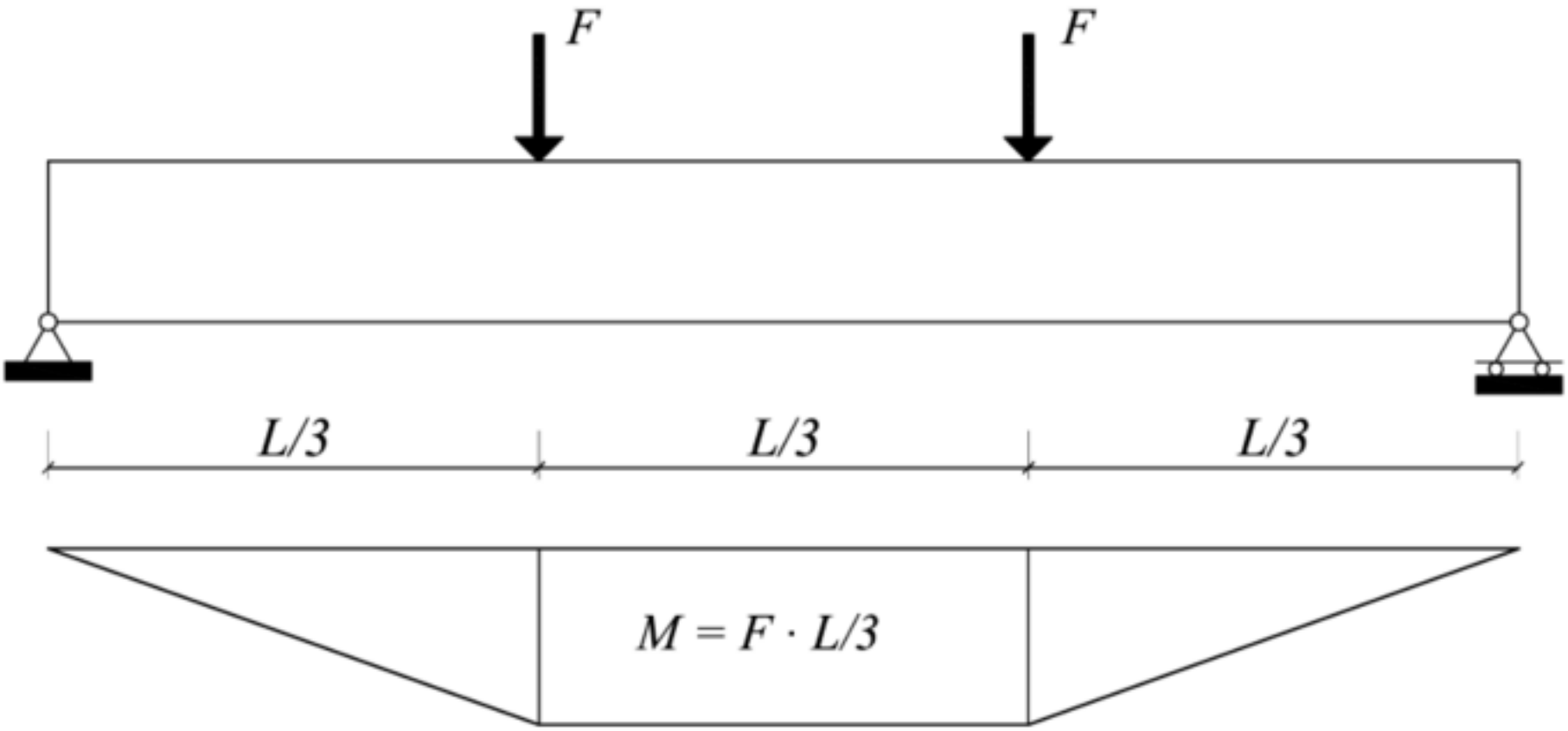

Figure 2

Click here to download high resolution image

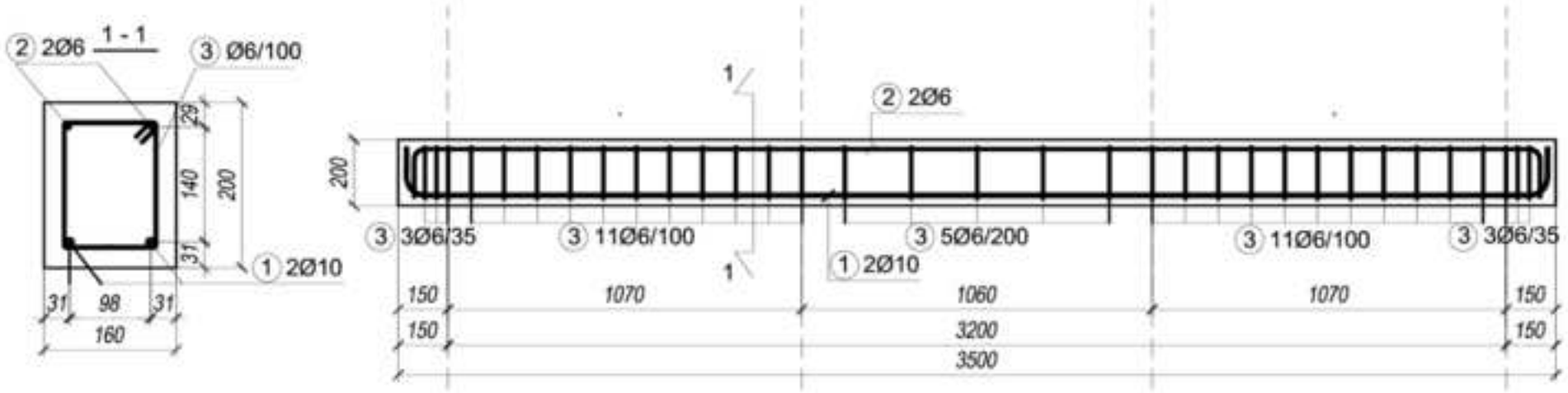

Figure 3

Click here to download high resolution image

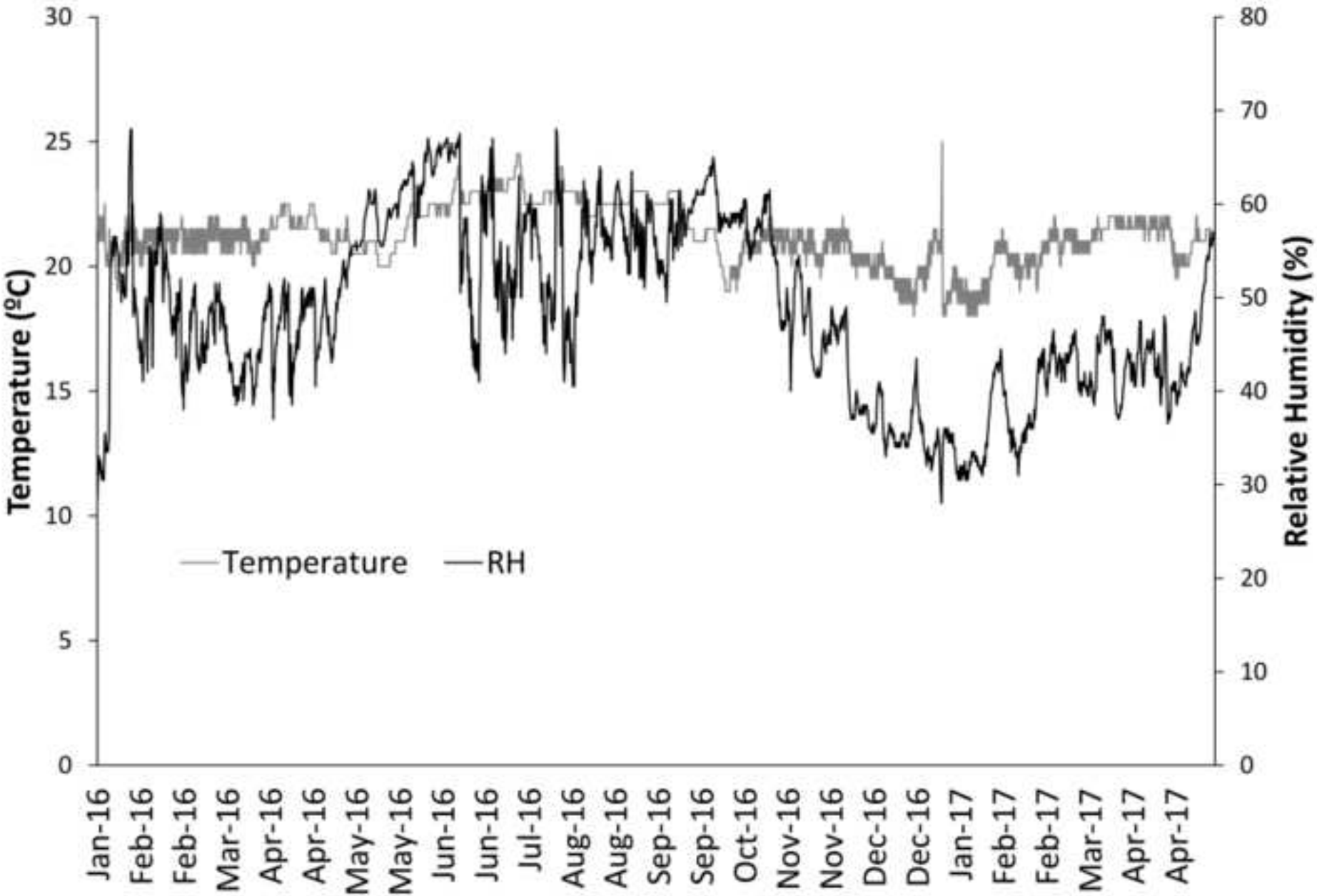

Figure 4

Click here to download high resolution image

Figure 5

Click here to download high resolution image

Figure 6

Click here to download high resolution image

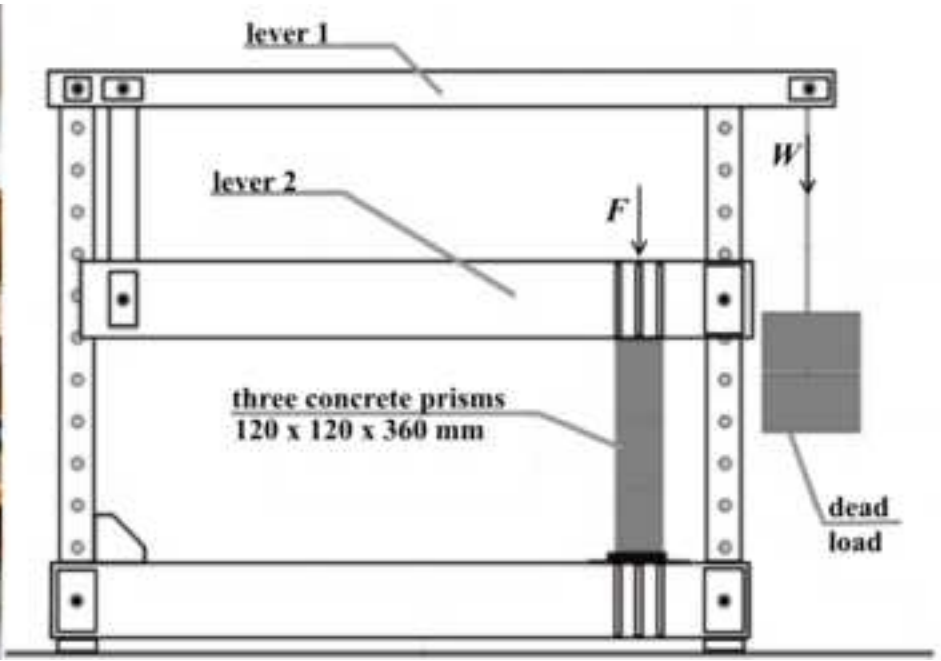

Figure 7
Click here to download high resolution image

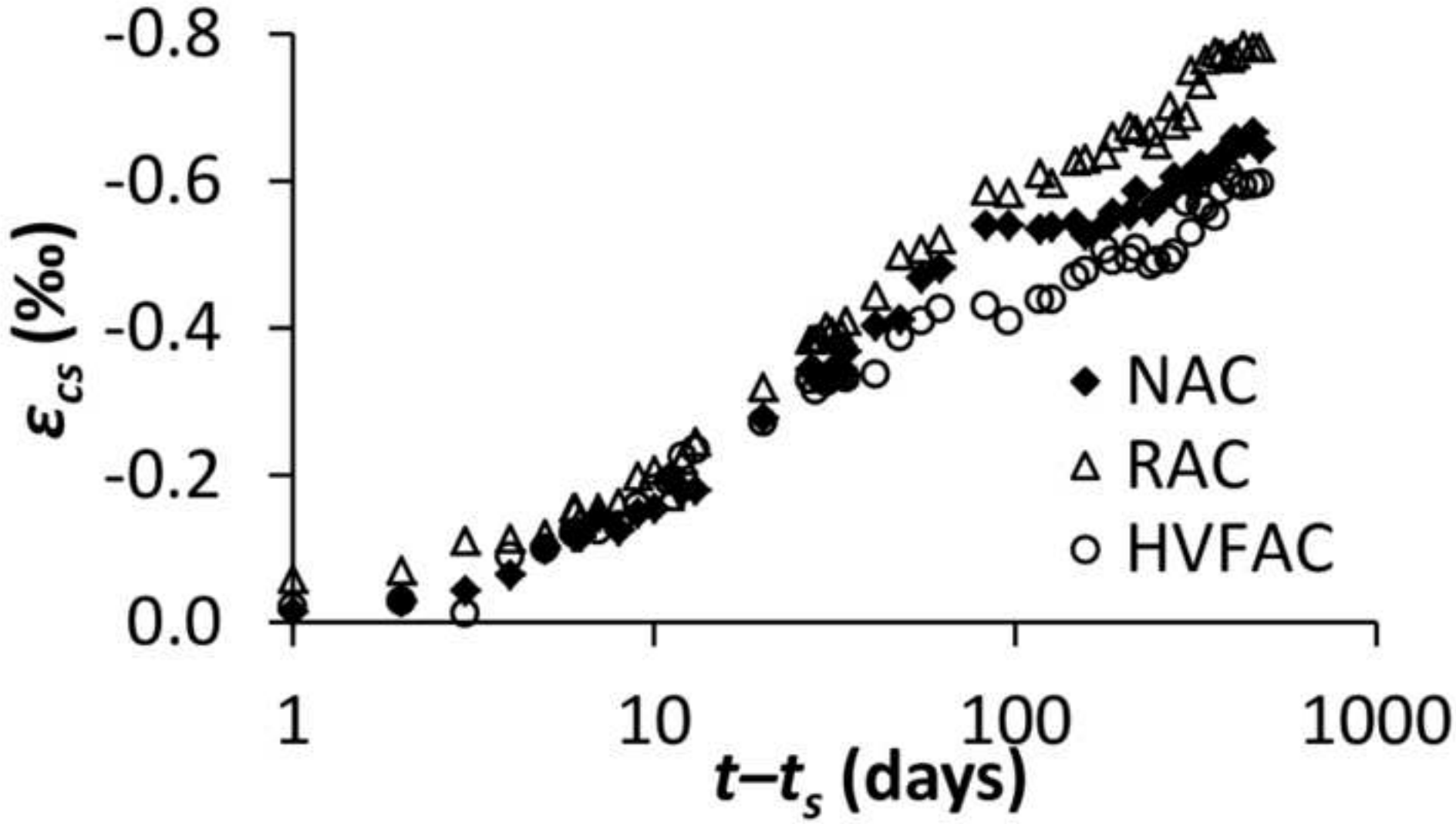

Figure 8

Click here to download high resolution image

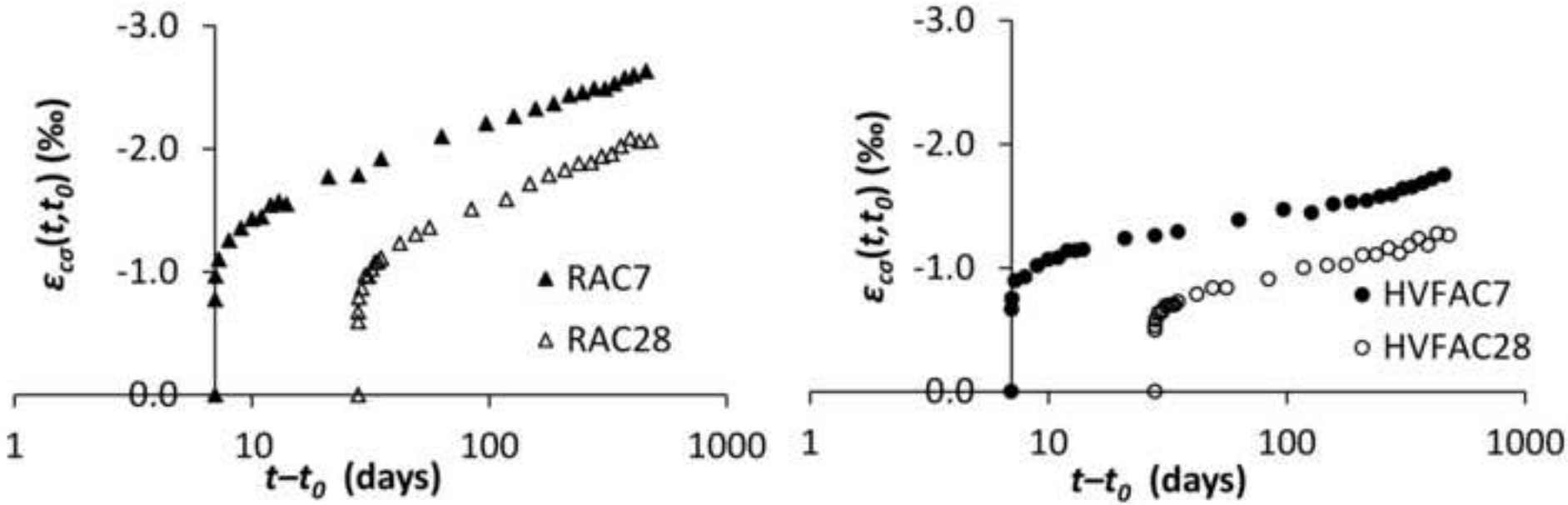

Figure 9

Click here to download high resolution image

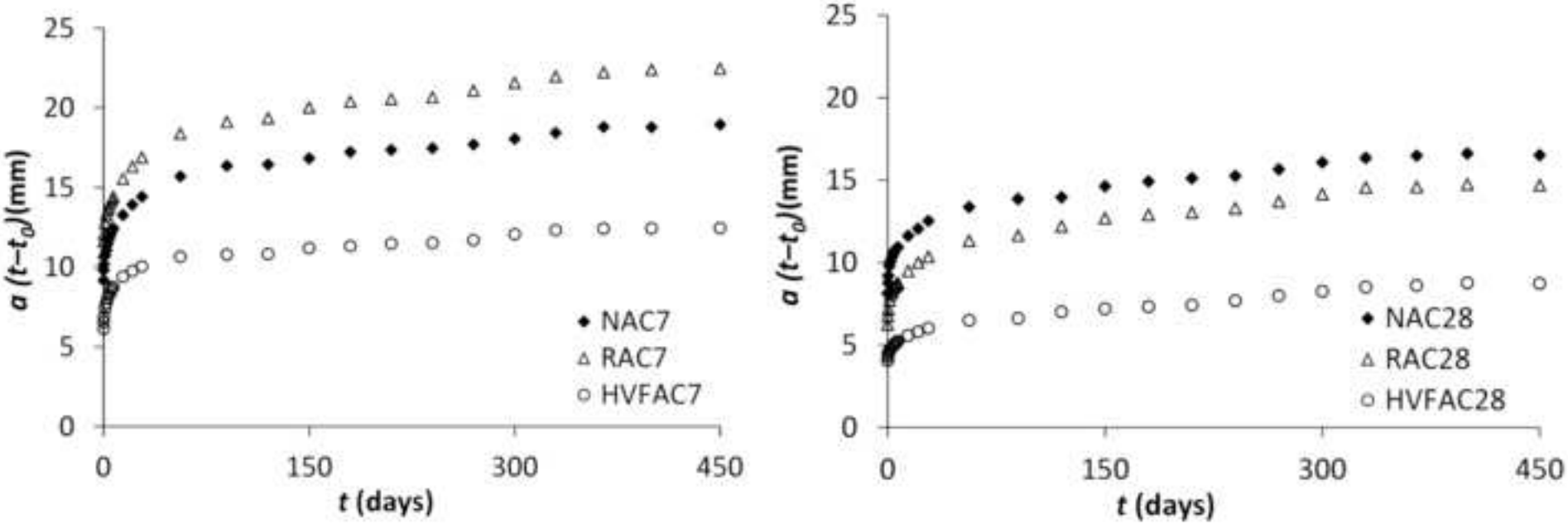

Figure 10

Click here to download high resolution image

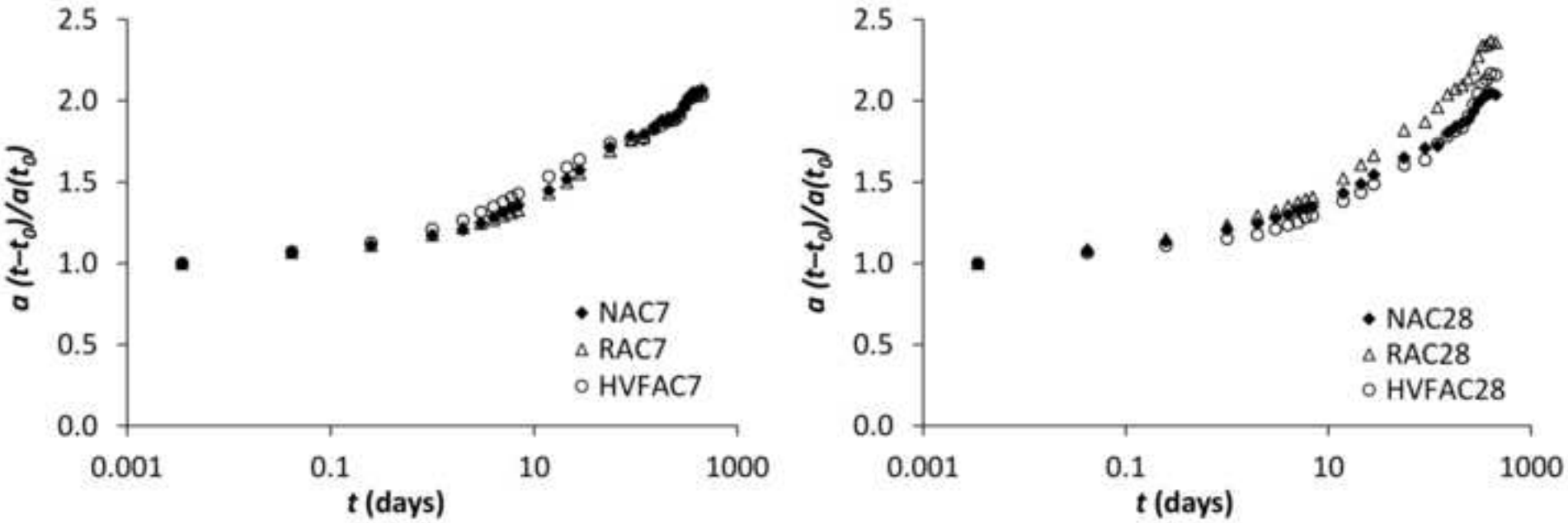

Figure 11

Click here to download high resolution image

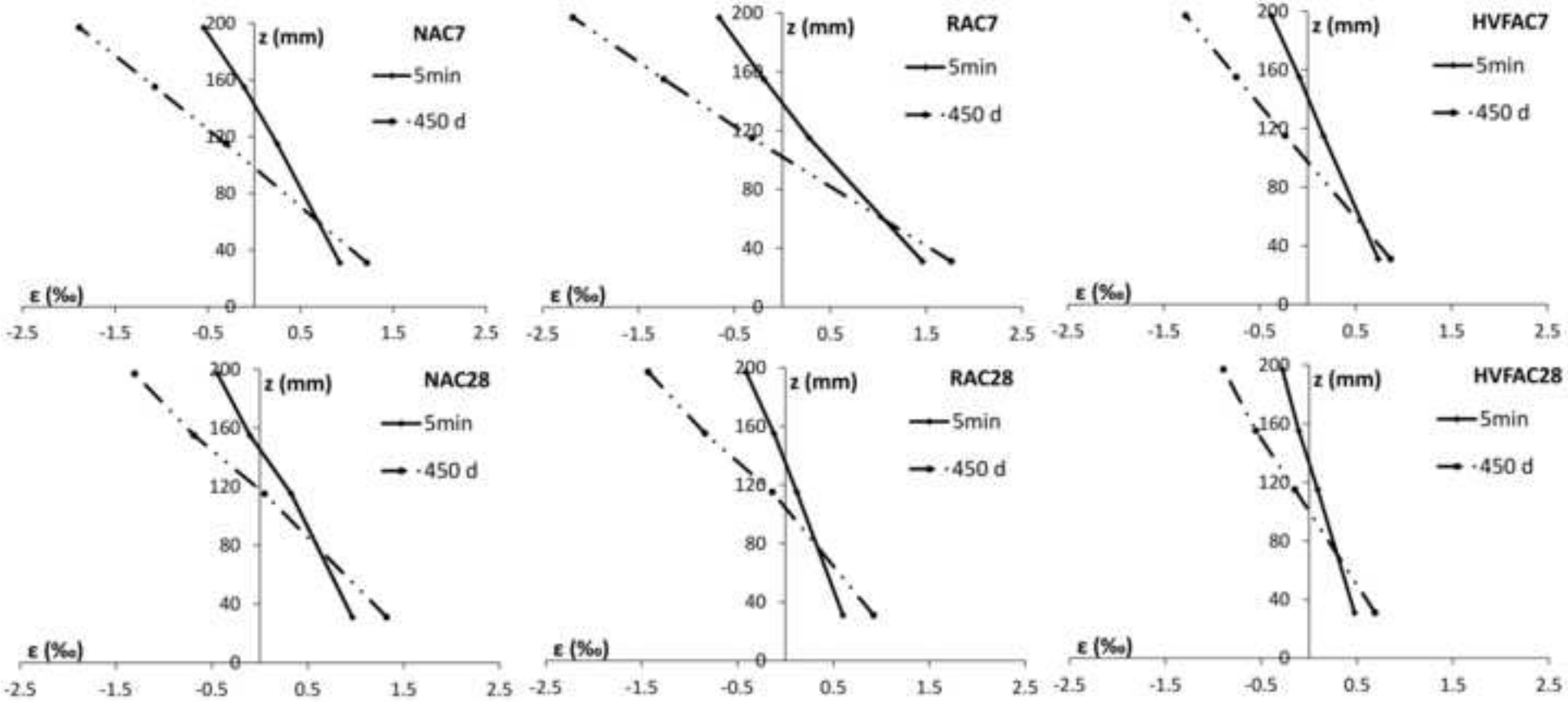

Figure 12

Click here to download high resolution image

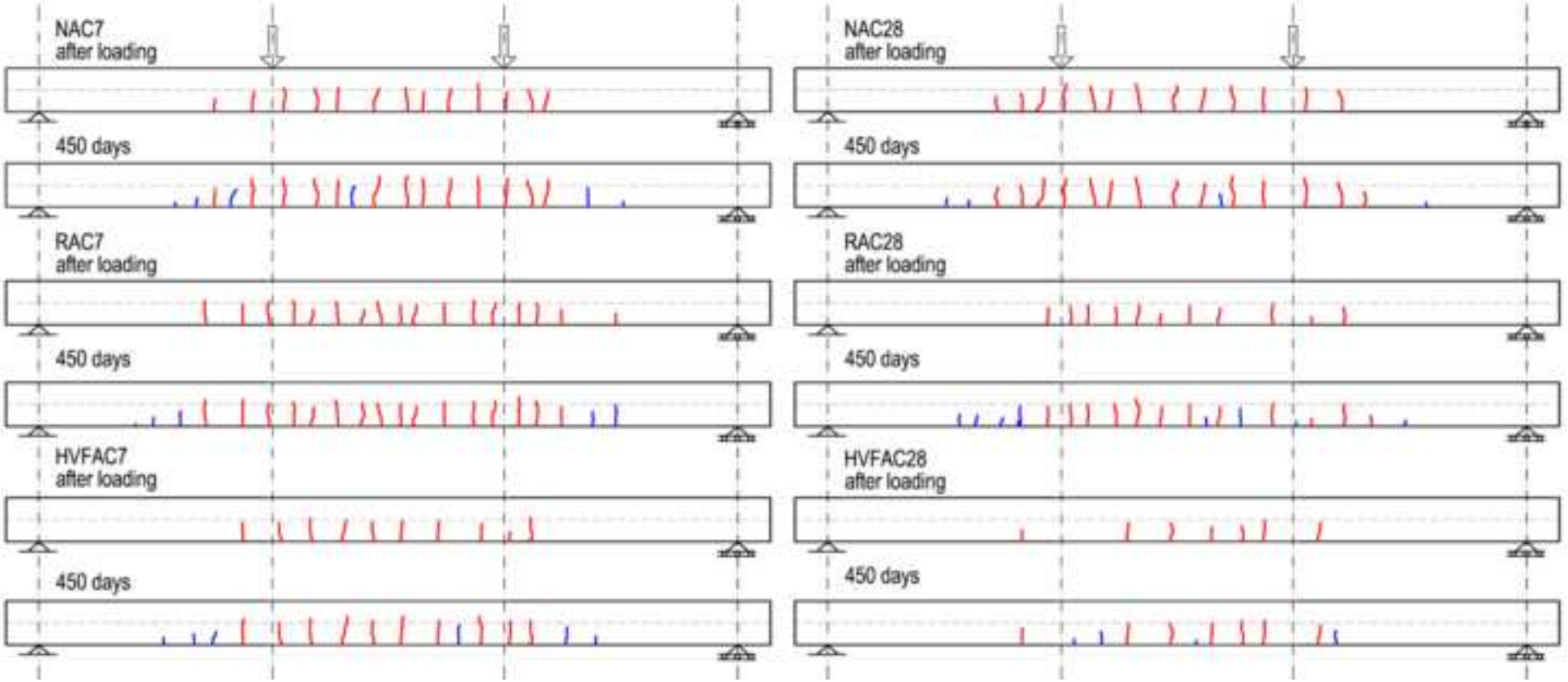

Figure 13
Click here to download high resolution image

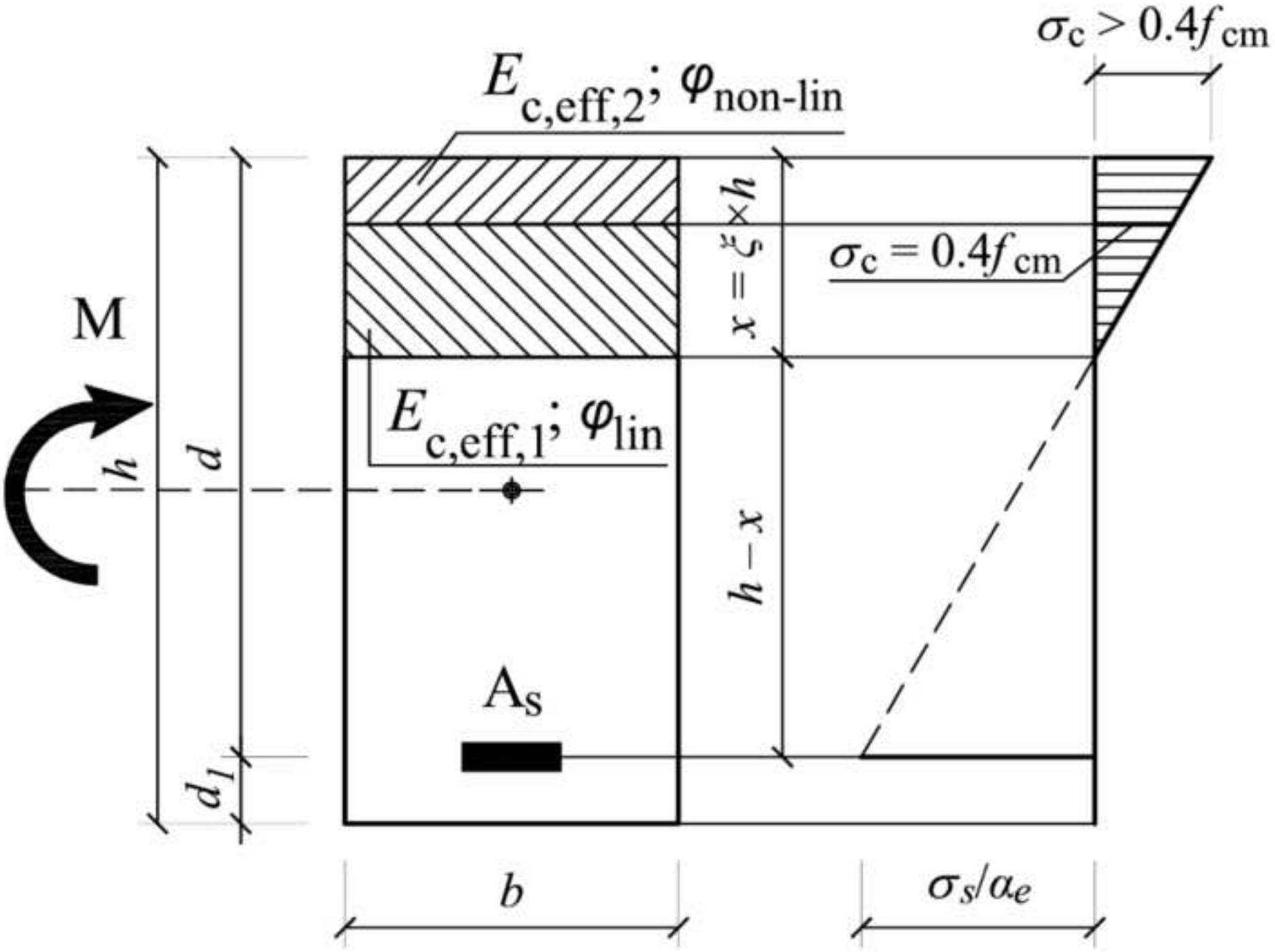

Figure 14

Click here to download high resolution image